Eur Radiol (2018) 28:348–355
DOI 10.1007/s00330-017-4942-5

NEURO

Noninvasive electrical conductivity measurement by MRI: a test of its validity and the electrical conductivity characteristics of glioma

Khin Khin Tha[1,2] · Ulrich Katscher[3] · Shigeru Yamaguchi[4] · Christian Stehning[3] · Shunsuke Terasaka[4] · Noriyuki Fujima[1] · Kohsuke Kudo[1,2] · Ken Kazumata[4] · Toru Yamamoto[5] · Marc Van Cauteren[6] · Hiroki Shirato[2,7]

Received: 30 March 2017 / Revised: 1 June 2017 / Accepted: 9 June 2017 / Published online: 11 July 2017

Abstract

Objectives This study noninvasively examined the electrical conductivity (σ) characteristics of diffuse gliomas using MRI and tested its validity.

Methods MRI including a 3D steady-state free precession (3D SSFP) sequence was performed on 30 glioma patients. The σ maps were reconstructed from the phase images of the 3D SSFP sequence. The σ histogram metrics were extracted and compared among the contrast-enhanced (CET) and noncontrast-enhanced tumour components (NCET) and normal brain parenchyma (NP). Difference in tumour σ histogram metrics among tumour grades and correlation of σ metrics with tumour grades were tested. Validity of σ measurement using this technique was tested by correlating the mean tumour σ values measured using MRI with those measured ex vivo using a dielectric probe.

Results Several σ histogram metrics of CET and NCET of diffuse gliomas were significantly higher than NP (Bonferroni-corrected $p \leq .045$). The maximum σ of NCET showed a moderate positive correlation with tumour grade ($r = .571$, Bonferroni-corrected $p = .018$). The mean tumour σ measured using MRI showed a moderate positive correlation with the σ measured ex vivo ($r = .518$, $p = .040$).

Conclusions Tissue σ can be evaluated using MRI, incorporation of which may better characterise diffuse gliomas.

Key Points

- *This study tested the validity of noninvasive electrical conductivity measurements by MRI.*
- *This study also evaluated the electrical conductivity characteristics of diffuse glioma.*
- *Gliomas have higher electrical conductivity values than the normal brain parenchyma.*
- *Noninvasive electrical conductivity measurement can be helpful for better characterisation of glioma.*

Keywords Electrical conductivity · Glioma · Magnetic resonance imaging · Steady-state free precession · Validity

Abbreviations and Acronyms

σ	Electrical conductivity
3D SSFP	3D steady-state free precession
CET	Contrast-enhanced tumour component
NCET	Non-contrast-enhanced tumour component
NP	Normal brain parenchyma
CSF	Cerebrospinal fluid
EPT	Electric properties tomography
σ_{EPT}	Electrical conductivity as measured by EPT
σ_{PROBE}	Electrical conductivity as measured by dielectric probe

Electronic supplementary material The online version of this article (doi:10.1007/s00330-017-4942-5) contains supplementary material, which is available to authorized users.

✉ Khin Khin Tha
kktha@med.hokudai.ac.jp

[1] Department of Diagnostic and Interventional Radiology, Hokkaido University Hospital, N-14, W-5, Kita-ku 060-8648 Sapporo, Japan

[2] Global Station for Quantum Medical Science and Engineering, Global Institution for Collaborative Research and Education, Hokkaido University, Sapporo, Japan

[3] Philips Research Laboratories, Hamburg, Germany

[4] Department of Neurosurgery, Faculty of Medicine, Hokkaido University, Sapporo, Japan

[5] Faculty of Health Sciences, Hokkaido University, Sapporo, Japan

[6] Clinical Science Philips Healthtech Asia Pacific, Tokyo, Japan

[7] Present address: Department of Radiation Medicine, Faculty of Medicine, Hokkaido University, Sapporo, Japan

RF	Radiofrequency
B_1	RF transmit magnitude
FLAIR	Fluid-attenuated inversion recovery
ε	Permittivity
Ω	Larmor frequency
Δ	Laplacian operator
H^+	Magnetic RF transmit field
μ	Magnetic permeability of the body
Φ^+	RF transmit phase
$\Phi^\pm$	RF transceive phase
ANOVA	Analysis of variance
ROC	Receiver-operating characteristic
AUC	Area under curve

Introduction

Electrical conductivity (σ) represents the ability of a material to conduct electric current and is determined mainly by the concentration and/or mobility of sodium ions in the material [1, 2]. Different materials are known to have different σ values, ranging from almost zero (insulators) to several million siemens per meter (S/m) (conductors). Living tissues also have variable σ values: fat and bone have lower σ values, whereas the cerebrospinal fluid (CSF) and blood have higher σ values [3]. Tumours, especially malignant ones, are reported to have higher σ values than do normal tissues [4].

The knowledge of σ differences between tumours and normal tissues has been applied in medicine for several decades [5]. Before the era of CT and MRI, surgeons used σ differences to localize brain tumours. By placing dielectric probes directly on the brain surface during craniotomies, differences in local tissue electrical impedance (i.e., the inverse of σ) could be identified between brain tumours and normal brain tissue [5]. The surgeons also came to notice the differences in electrical impedance among different types of brain tumours through these procedures, which suggests the possible usefulness of the information about electrical properties in distinguishing brain tumours.

Information about electric properties can also be obtained from MRI, due to the relationship between electricity and magnetism [6]. Haacke et al. were the first to attempt the derivation of electric properties from the measurable magnetic field, using the Helmholtz equation [7]. This effort was followed by further investigations and improvements by other researchers [8, 9], which led to the estimation of tissue σ values noninvasively and in vivo from the phase maps of MRI scans, a technique termed electric properties tomography (EPT) [6]. Although any other phase maps can be used to calculate σ, EPT typically uses the phase images of a 3D steady-state free precession (3D SSFP) sequence to minimize the effect of B_1 magnetic field inhomogeneities and unwanted phase contributions from flow, motion, and eddy currents in the tissues [6]. EPT represents an improvement over previous techniques because it is completely noninvasive [8, 9].

The validity of EPT for σ measurement has been tested by comparing the σ values measured by EPT and dielectric probes for saline phantoms containing different saline concentrations [10]. Very high correlation is observed between the two, indicating the validity of EPT for noninvasive σ estimation. However, to our knowledge, no comparison between EPT and dielectric probe of σ in living tissues has been reported. This comparison is important because results from saline phantom measurements cannot be directly applied to living tissues. Regarding the estimation of σ in living tissues by EPT, previous studies have reported on the σ_{EPT} characteristics of normal brain tissues [11, 12]. In agreement with the literature, these reports observe that the σ of the CSF is higher than that of the normal grey matter, which in turn has a higher σ than that of normal white matter [3]. The clinical applicability of EPT has also been documented in breast and cervical cancers [13, 14]. However, its usefulness in other diseases or body regions has not been well explored.

This study tested the validity of noninvasive σ measurement by EPT by correlating the σ of brain tumours measured in vivo by EPT (σ_{EPT}) with that measured ex vivo by a dielectric probe (σ_{PROBE}). The σ characteristics of diffuse gliomas were also examined using EPT to evaluate if noninvasive σ measurements could be useful in grading these tumours.

Materials and methods

Patients

This retrospective study was approved by the local institutional review board. Written informed consent for contrast-enhanced MR examination was obtained from all patients. EPT was performed as a part of the routine protocol, and the magnitude images were used to obtain morphological information on brain tumours. The requirement of written informed consent for EPT was waived.

MR images of patients with diffuse gliomas were collected from our hospital database. The recruitment period was 35 months (February 2013 through December 2015), and the inclusion criterion was the diagnosis of diffuse gliomas. Diagnoses were principally made by histological confirmation (i.e., the hospital pathology reports were referred for the final diagnoses). In patients who did not undergo surgery or biopsy, diagnoses were obtained by hospital radiology reports made at or closest to the time of EPT imaging. We included only those patients in whom MRI and PET imaging (one or more of the following: ^{18}F-fludeoxyglucose-PET, ^{11}C-methionine-PET, and ^{18}F-fluoromisonidazole-PET) reports suggested the same

tumour grade. For both histological and radiological grading, tumour grades were determined in accordance with the WHO classifications [15]. The exclusion criteria were any prior treatment, equivocal or unconfirmed diagnosis, failure to acquire the 3D SSFP sequence, and visible artefacts on the phase maps of the 3D SSFP sequence.

Of 72 possible patients, 42 were excluded for prior treatments such as tumour debulking surgery, radiation, or chemotherapy (n = 15); equivocal or unconfirmed diagnoses (n = 5); lack of a 3D SSFP sequence (i.e., scans were performed with scanners incapable of 3D SSFP imaging or patients failed to complete the MRI protocol) (n = 21); and visible motion-induced ghosting artefacts on the phase maps of the 3D SSFP sequence (n = 1). Thirty patients (mean age ± standard deviation = 50.73 ± 18.21 years, age range = 12–84 years; 14 men and 16 women; eight grade II, 11 grade III, and 11 grade IV tumours) eligible for this study (Fig. 1). A summary about patient characteristics is given in Table 1.

Ex vivo σ measurement

Pieces of the resected tumour tissues of patients who underwent subsequent surgery or biopsy were used for ex vivo σ measurement. From 30 patients, 16 tumour samples (three grade II, four grade III, and nine grade IV tumours) were available. These samples were initially stored in a frozen state (-80 °C) at the Department of Neurosurgery of the institution and were thawed to room temperature (the mean water temperature ± standard deviation = 23.21 ± 0.59 °C), just before the measurement of σ_{PROBE} values. A dielectric probe (N1500A, Keysight Technologies, USA) and an analyser (N9918A, Keysight Technologies, USA) were used to measure σ_{PROBE}. All measurements were done by a researcher trained for σ_{PROBE} measurement. Five measurements were conducted for each tumour sample, and the mean value was used. To remove observer bias, the σ_{EPT} values and histological information about the samples were blinded to the researcher who performed the measurements.

MRI

EPT was conducted using a 3D SSFP sequence taken with nonselective radiofrequency (RF) pulses and a 3 T-MR imager (Achieva TX, Philips Medical Systems, Best, the Netherlands). A standard 32-channel RF head coil (Philips Medical Systems, Best, the Netherlands) was used for signal reception. The SSFP images were divided by the sensitivity profile of this RF coil, which was measured using a built-in pre-scan, to remove unwanted image contributions. The scan parameters were: repetition time/echo time/flip angle/number of excitation = 3.5 ms/1.7 ms/25°/2, acquisition voxel size = 1.3 × 1.2 × 1 mm^3, reconstructed voxel size = 0.98 × 0.98 × 1 mm^3, slice orientation = sagittal, acquisition time = 3 min 40 s. The σ_{EPT} maps were calculated essentially as the second spatial derivative from three dimensions of the phase maps, implemented by in-house software written in the C programming language. The details are described in the "Electronic supplementary material" section.

In addition to EPT, axial pre- and postcontrast-enhanced T1-weighted imaging, T2-weighted imaging, and fluid-attenuated inversion recovery (FLAIR) imaging were also conducted. All MRI sequences, except postcontrast-enhanced T1-weighted imaging, were acquired before contrast administration. Image quality was assured throughout the study by ruling out any variation in magnetic field homogeneity, coil sensitivity profile, and artefacts in daily phantom scans performed by an experienced technologist. Since the phase information of image data is particularly important in this study, we also made sure that there were no issues regarding this by performing susceptibility-weighted imaging, which is highly sensitive to phase. All MRI measurements were performed under the normal operating mode, and the specific absorption rate was kept below 3.2 W/kg/10 min [16].

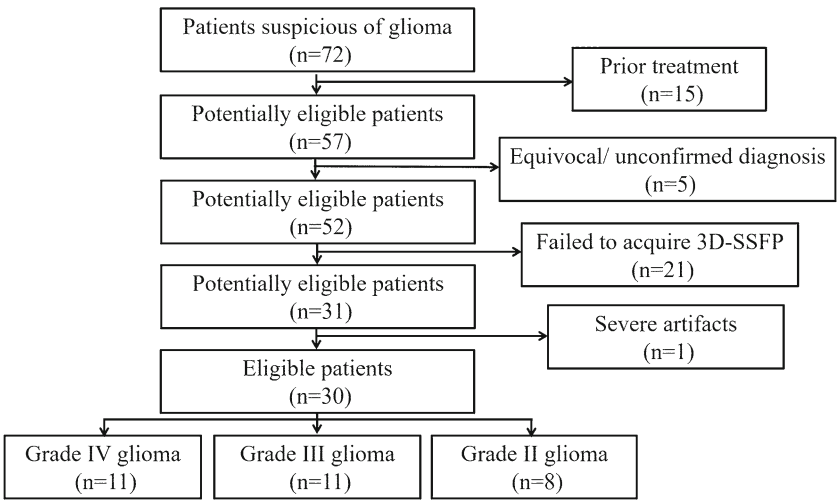

Fig. 1 Flow diagram showing selection of patients

Table 1 Summary of the characteristics of the patients

Tumour grade*	No.	Men:Women	Mean age ± Standard deviation (Range)	Pathological diagnosis	Radiological diagnosis
Grade IV	11	8:3	63.18 ± 16.99 (42-84) years	10 (glioblastoma)	1 (glioblastoma)
Grade III	11	2:9	43.36 ± 17.47 (12-69) years	11 (6 anaplastic astrocytoma, 3 anaplastic oligodendroglioma, 1 anaplastic oligoastrocytoma, 1 anaplastic ependymoma)	0
Grade II	8	4:4	43.67 ± 11.89 (33-67) years	6 (2 diffuse astrocytoma, 2 oligodendroglioma, 2 oligoastrocytoma)	2 (low grade glioma)

* according to the World Health Organization (WHO) classification

Image processing

Image processing involved segmentation of the contrast-enhanced tumour component (CET), noncontrast-enhanced tumour component (NCET), and the normal brain parenchyma (NP) of each patient, for measurement of the σ_{EPT} values. This process included image coregistration (SPM12, Wellcome Trust Centre for Neuroimaging, University College of London, Oxford, UK); determination of the signal intensity range for CET, NCET, and NP (MRICron Version 1, www.mricro.com); and erosion (Image J 1.50i, National Institutes of Health, Bethesda, MD, USA). Segmentation of the resected tumour area was also performed in patients for which tumour samples were available to compare the σ_{EPT} and σ_{PROBE} values. These steps are detailed in Fig. 2 and the "Electronic supplementary material" section.

Image evaluation

The validity of noninvasive σ measurements by EPT was tested by correlating the mean σ_{EPT} of the resected tumour area with the ex vivo σ_{PROBE} value. Pearson's product-moment correlation analysis was used for this purpose. To represent better the σ characteristics of each tumour component, histogram analysis was used to evaluate the σ_{EPT} values. For each tumour component and NP, the mean, minimum, maximum, mode, quartiles, skewness, and kurtosis of the σ_{EPT} values were derived (Image J 1.50i). The differences in σ_{EPT} among the CET, NCET, and NP were tested using one of the following testing approaches: repeated-measures analysis of variance (ANOVA) and post hoc Bonferroni tests, Friedman and post hoc Wilcoxon signed-rank tests, or paired t-tests. Different approaches were chosen based on the normality of data distribution and the number of levels formed by

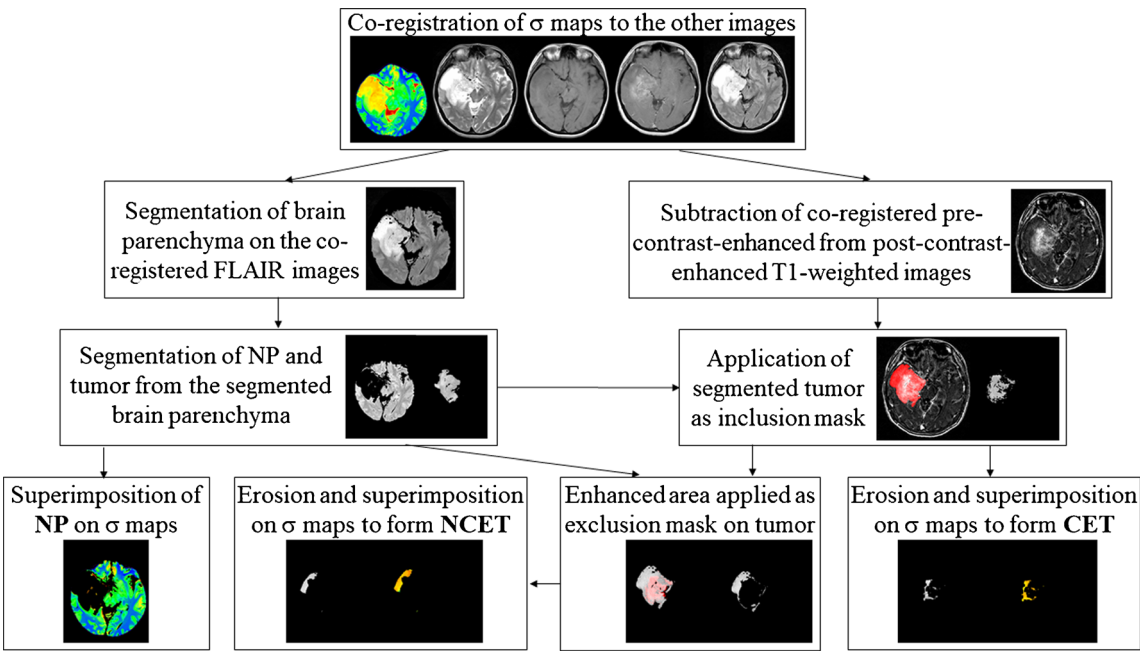

Fig. 2 Summary of image processing steps. NP, NCET, and CET indicate the normal brain parenchyma, noncontrast-enhanced tumour component, and contrast-enhanced tumour component, respectively

the variables. Repeated-measures ANOVA and post hoc Bonferroni tests were used when the data were normally distributed and had three levels (CE, NCE, and NP). Friedman and post hoc Wilcoxon signed-rank tests were used when the data were not normally distributed but had three levels. Paired t-tests were used for normally-distributed data with only two levels (i.e., CE and NP or NCE and NP only). The σ_{EPT} values were also tested for correlation with tumour grade using Pearson's product-moment correlation analysis. The accuracy of EPT in distinguishing glioma grades was then compared with that of radiologists using routine MRI findings (radiological reports) through receiver-operating characteristic (ROC) analyses. For all analyses, a Bonferroni-corrected $p < .050$ was considered statistically significant. Statistical analyses were performed by using SPSS version 14.0 (IBM, Armonk, NY, USA).

Results

Validity of noninvasive σ measurement by EPT

The mean σ_{EPT} of the resected tumour area showed a moderate positive correlation with the σ_{PROBE} values measured ex vivo (r = .518, $p = .040$) (Fig. 3).

Glioma σ_{EPT} values

The representative σ_{EPT} maps of grade II to grade IV gliomas and the corresponding postcontrast-enhanced T1-weighted and FLAIR images are shown in Fig. 4a, b, and c. The mean values of the σ_{EPT} histogram metrics are summarized in Table 2. For the grade IV tumours, the mean σ_{EPT} values significantly differed among the CET, NCET, and NP. CET showed the highest values, followed in descending order by NCET and NP (Bonferroni-corrected $p \leq .015$). The maximum, median, mode, and 25th and 75th percentiles of both CET and NCET were significantly higher than those of NP (Bonferroni-corrected $p < .003$). For the grade III tumours, the maximum and 75th percentile of both NCET and CET were significantly higher than those of NP (Bonferroni-corrected $p \leq .045$). The mean, median, and 25th percentile of the σ_{EPT} of NCET were significantly higher than those of NP (Bonferroni-corrected $p \leq .042$). The mean and median σ_{EPT} of CET tended to be higher than those of NP (Bonferroni-corrected $p \leq .060$). Statistical comparison of the σ_{EPT} of CET with those of NCET and NP was impossible for the grade II tumours due to an insufficient number of tumours with contrast enhancement (n = 1). The mean, median, mode, minimum, maximum, and the 25th and 75th percentiles of NCET were significantly higher than those of NP (Bonferroni-corrected $p \leq .008$). Among the tumour grades, the maximum and 75th percentile of NCET in the grade IV tumours were significantly higher than those in the grade II tumours (Bonferroni-corrected $p \leq .036$). The maximum, median, and 75th percentile of CET in the grade IV tumours were significantly higher than those in the grade III tumours (Bonferroni-corrected $p \leq .040$).

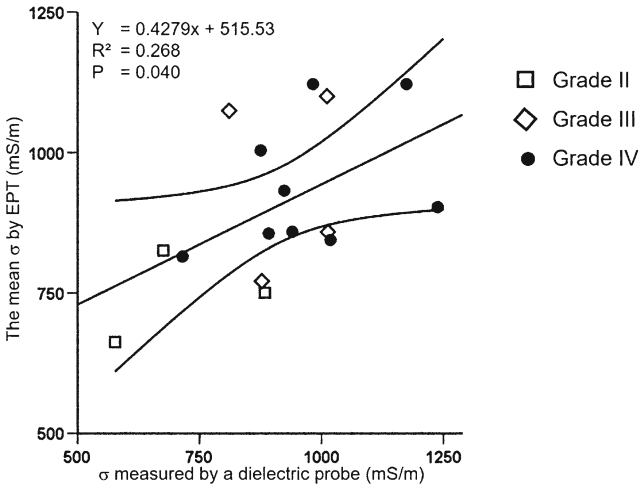

Fig. 3 Scatterplots showing correlation between the mean electrical conductivity (σ) value of the resected tumour area measured noninvasively by electric properties tomography (EPT) and that by a dielectric probe. The straight and curved lines indicate the mean and 95% confidence interval

Correlation of σ_{EPT} with tumour grade

The maximum σ_{EPT} of NCET showed significant moderate positive correlation with tumour grade (r = .571, Bonferroni-corrected $p = .018$). The 75th percentile of NCET tended to show a moderate positive correlation with tumour grade (r = .534, Bonferroni-corrected $p = .054$).

Accuracy of EPT in distinguishing glioma grades

The maximum σ_{EPT} of CET {area under curve (AUC) = .833, $p = .027$}, as well as the maximum (AUC = .894, $p = .009$) and the 75th percentile (AUC = .894, $p = .009$) of NCET, could distinguish the grade IV tumours from the other tumour grades. Each aforementioned metric was more accurate in distinguishing grade IV tumours from lower-grade gliomas (AUC = 1.000, $p = .046$) than was preoperative MRI grading by radiologists (AUC = .750, $p = .317$) (n = 15).

Discussion

To our knowledge, this is the first study to examine the validity of noninvasive σ measurements by using MRI and the σ_{EPT} characteristics of diffuse gliomas. We used all of the major histogram metrics, instead of only the mean values, to

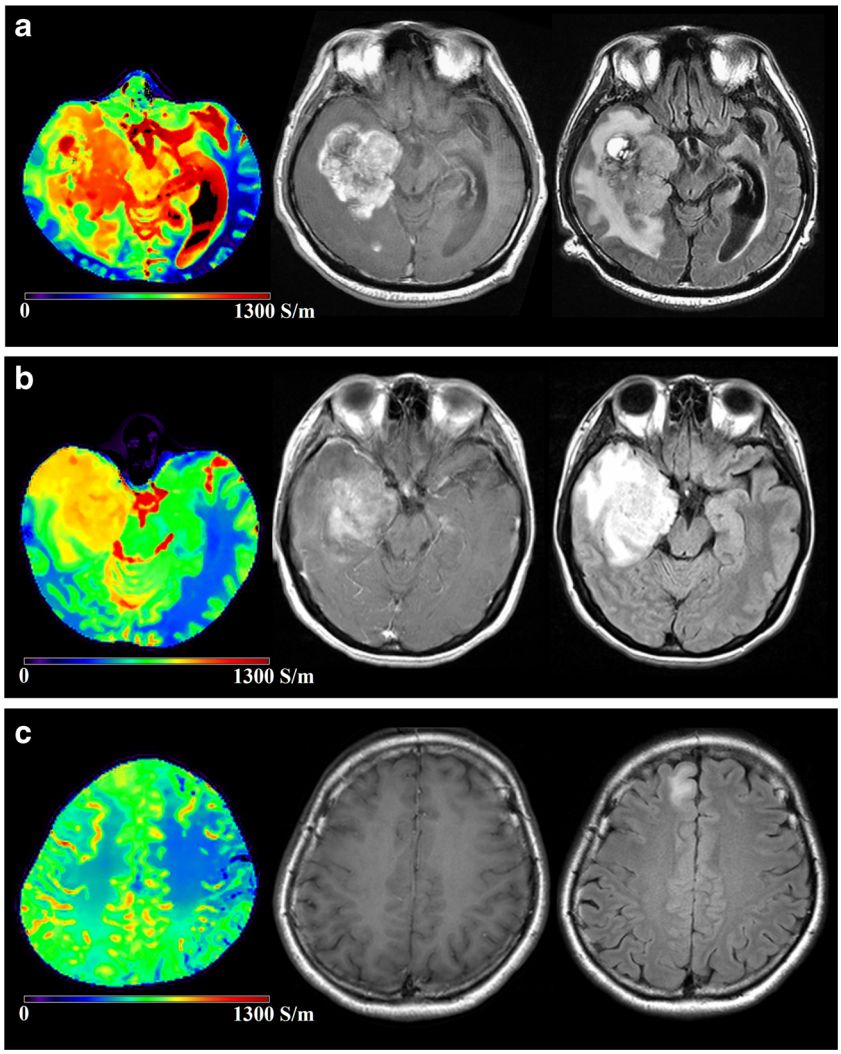

Fig. 4 The electrical conductivity (σ_{EPT}) maps and the corresponding postcontrast-enhanced T1-weighted and FLAIR images of a (**a**) grade IV glioma, (**b**) grade III glioma, and (**c**) grade II glioma. The unit of σ_{EPT} is millisiemens per meter (mS/m)

characterise better the σ_{EPT} values [17]. Our results indicate that EPT can be used to estimate the tissue σ values. This σ_{EPT} information can help better characterise diffuse gliomas and differentiate tumour grades.

The mean σ_{EPT} of resected tumour area showed a moderate positive correlation with the σ_{PROBE} values. However, a previous experiment using saline phantoms found an excellent correlation between σ_{EPT} and σ_{PROBE} values [10]. This difference may be attributed to the different natures of the two studies. The former compared σ between the in vivo and ex vivo tissues, whereas the latter was conducted under an experimental setting. The σ values are generally thought to be influenced by tissue sodium ion concentration and mobility [1, 2]. Ion mobility may have been altered in the resected tumour samples, resulting in a change in the σ_{PROBE} values. The difference in the temperatures at which measurements were conducted—body temperature (approximately 37 °C) for the in vivo measurements and room temperature (23.21 ± 0.59 °C) for the ex vivo measurements—may also be responsible. Generally, σ increases with temperature by approximately 2%/°C [18]. However, this global scale, if taken into account, would not change the observed correlation between the σ_{EPT} and σ_{PROBE} values. Freezing and thawing might also have affected the σ_{PROBE} values because sodium concentration has been reported to differ between the two conditions [19], although our results from chicken breast phantoms frozen to -80 °C then thawed to room temperature did not reveal any significant difference in σ_{PROBE} values between the two temperatures (results not shown). Additionally, the ex vivo measurements were performed only on a piece of resected tumour, whereas the in vivo measurements included the entire resected tumour area, which may explain the disparity of σ values between EPT and dielectric probe measurements. Finally, σ_{EPT} values are often subjected to boundary errors and B_0 magnetic field inhomogeneities [20], which are more prominent in living subjects.

The σ_{EPT} values of CET and NCET in gliomas were significantly higher than those of NP, suggesting the possible

Table 2 The σ_{EPT} values of CET, NCET, and NP of each grade of glioma. The mean ± standard deviations are given for each histogram metric. * and + indicate statistical significance (Bonferroni-corrected $p < .050$) among CET, NCET, and NP of each tumour grade. Bolded and italic numbers indicate statistical significance (Bonferroni-corrected $p < .050$) among tumour grades

	Grade IV			Grade III			Grade II		
	CE (n = 11)	NCE (n = 11)	NP (n = 11)	CE (n = 6)	NCE (n = 10)	NP (n = 11)	CE (n = 1)	NCE (n = 8)	NP (n = 8)
Mean	950.97 ± 135.12^{*+}	898.26 ± 142.24^{*+}	471.15 ± 41.68^{*+}	808.21 ± 126.59*	784.08 ± 145.70^{+}	466.78 ± 57.57^{*+}	1076.77 ± NA	795.27 ± 102.26^{+}	473.29 ± 31.96^{+}
Minimum	572.92 ± 151.62	486.17 ± 186.78	447.13 ± 48.90	589.61 ± 180.88	487.70 ± 153.18	444.99 ± 56.26	991.40 ± NA	578.75 ± 109.01^{+}	447.34 ± 39.43^{+}
Maximum	**1243.06 ± 186.52***	*1239.66 ± 152.92*$^{+}$	502.21 ± 35.95^{*+}	**963.35 ± 174.80***	1068.21 ± 201.15^{+}	491.45 ± 54.04^{*+}	1120.45 ± NA	*969.03 ± 132.57*$^{+}$	495.02 ± 39.98^{+}
Mode	998.50 ± 150.24*	927.20 ± 132.87^{+}	481.60 ± 51.31^{*+}	847.90 ± 188.48	797.79 ± 190.52	466.96 ± 62.96	1093.94 ± NA	803.78 ± 174.91^{+}	472.72 ± 27.38^{+}
25th percentile	797.99 ± 141.23*	765.03 ± 114.59^{+}	461.15 ± 43.57^{*+}	709.03 ± 135.62	687.58 ± 130.12	457.46 ± 53.45	1024.41 ± NA	709.56 ± 61.38^{+}	460.45 ± 33.98^{+}
Median	970.07 ± 153.93*	*952.41 ± 106.89*$^{+}$	475.35 ± 39.81^{*+}	804.96 ± 133.57*	835.15 ± 149.95^{+}	470.38 ± 51.37^{*+}	1057.43 ± NA	*733.30 ± 60.14*$^{+}$	474.61 ± 32.45^{+}
75th percentile	1114.97 ± 169.95*	*1106.89 ± 120.22*$^{+}$	488.92 ± 37.20^{*+}	888.23 ± 150.72*	959.13 ± 175.81^{+}	483.30 ± 49.95^{*+}	1089.44 ± NA	*907.08 ± 89.40*$^{+}$	488.15 ± 33.76^{+}
Skewness	0.00 ± 0.00	0.00 ± 0.00	0.00 ± 0.00	0.00 ± 0.00	0.00 ± 0.00	0.00 ± 0.00	0.00 ± NA	0.00 ± 0.00	0.00 ± 0.00
Kurtosis	(-1.20) ± 0.00	(-1.20) ± 0.00	(-1.20) ± 0.00	(-1.20) ± 0.00	(-1.20) ± 0.00	(-1.20) ± 0.00	(-1.20) ± NA	(-1.20) ± 0.00	(-1.20) ± 0.00

utility of σ_{EPT} for identifying different tumour compartments. A previous study on sodium MR imaging of brain tumours observed increased sodium concentrations in gliomas compared to those in NP [21]. Our observation of increased σ_{EPT} values in diffuse gliomas is also thought to reflect increased sodium ion concentrations within the tumours [2]. As proposed by the previous report [21], increased tumour sodium content may be due to increases in the intracellular sodium within rapidly proliferating tumour cells and/or the extracellular sodium within the interstitial space that enters tumours through the defective blood–brain barrier. The destruction of myelin, which serves as an insulator of electric current, and neovascularisation may also contribute [11, 22, 23]. The observation of higher mean σ_{EPT} values for CET than for NCET in the grade IV tumours suggests that the CET contains more rapidly proliferating tumour cells than does NCET. The flux of extracellular sodium to the tumour through the defective blood–brain barrier may also be responsible [24].

Several σ_{EPT} histogram metrics differed significantly among the three tumour grades. The maximum σ_{EPT} of NCET also showed a moderate positive correlation with tumour grade. These findings suggest the potential usefulness of σ_{EPT} in grading diffuse gliomas. Higher σ_{EPT} values in higher-grade gliomas may be due to higher sodium ion concentrations within the tumours. This finding agrees with the observation that tissue sodium content is higher in the rapidly proliferating cells [21]. The role of ion mobility on the σ_{EPT} characteristics is less clear. Although ion mobility may increase in higher-grade gliomas due to necrosis and the disruption of cell membranes, which hinder molecular motion, ion mobility may also be limited by increased tumour cell density [25]. This issue should be clarified in future research.

A few limitations must be addressed. First, to obtain more reliable results, identical pieces of tumour tissue should be used to measure both σ_{PROBE} and σ_{EPT}. While this flaw is an unavoidable limitation of a retrospective study, our results suggest the potential utility of EPT for noninvasive measurement of the σ values of living tissues. Second, the sample size for each grade of glioma is small. This situation prevented the comparison of σ_{EPT} between CET and NCET or NP for grade II gliomas. Further studies with larger sample sizes are warranted to confirm our results.

In conclusion, this preliminary study demonstrated the validity of EPT and its potential usefulness in the evaluation of diffuse gliomas. Possible acquisition of EPT with scanners capable of 3D SSFP sequence without the need for specially designed head coils and provision of a new image contrast based on the σ characteristics may also be the additional values for EPT. The physiological background of tissue σ values requires further investigation.

Acknowledgements The authors wish to thank Dr. Yoichi M Ito, Department of Biostatistics, Faculty of Medicine, Hokkaido University, for kind advice on statistics and Dr. Thomas Stehle, Philips Research Laboratories, Germany, for kind contribution of brain segmentation algorithm.

Compliance with ethical standards

Guarantor The scientific guarantor of this publication is Khin Khin Tha.

Conflict of interest Three authors of this manuscript (Ulrich Katscher, Christian Stehning, Marc Van Cauteren) declare relationships with the following company: Philips.

Funding This study has received funding by the Grant-in-aid for scientific research by the Japan Society for Promotion of Science (KAKENHI-26461817), Global Institution for Collaborative Research and Education, Hokkaido University, and Philips Electronics, Japan.

Statistics and biometry Dr. Yoichi M Ito kindly provided statistical advice for this manuscript.

Informed consent Written informed consent was waived by the Institutional Review Board.

Ethical approval Institutional Review Board approval was obtained.

Methodology
- retrospective
- diagnostic or prognostic study/experimental
- performed at one institution

References

1. Kandadai MA, Raymond JL, Shaw GJ (2012) Comparison of electrical conductivities of various brain phantom gels: developing a 'Brain Gel Model'. Mater Sci Eng C Mater Biol Appl 32:2664–2667
2. van Lier AL, de Bruin PW, Aussenhofer SA et al (2013) 23Na-MRI and EPT: Are sodium concentration and electrical conductivity at 298 MHz (7T) related? [abstract]. Proc Intl Soc Mag Reson Med 21:115
3. Gabriel C, Peyman A, Grant EH (2009) Electrical conductivity of tissue at frequencies below 1 MHz. Phys Med Biol 54:4863–4878
4. Lu Y, Li B, Xu J, Yu J (1992) Dielectric properties of human glioma and surrounding tissue. Int J Hyperth 8:755–760
5. Organ L, Tasker RR, Moody NF (1968) Brain tumor localization using an electrical impedance technique. J Neurosurg 28:35–44
6. Katscher U, Kim DH, Seo JK (2013) Recent progress and future challenges in MR electric properties tomography. Comput Math Methods Med 2013:546562
7. Haacke EM, Pepropoulos LS, Nilges EW, Wu DH (1991) Extraction of conductivity and permittivity using magnetic resonance imaging. Phys Med Biol 36:723–734
8. Joy ML, Scott GC, Henkelman RM (1989) In vivo detection of applied electric currents by magnetic resonance imaging. Magn Reson Imaging 7:89–94
9. Seo JK, Yoon JR, Woo EJ, Kwon O (2003) Reconstruction of conductivity and current density images using only one component of magnetic field measurements. IEEE Trans Biomed Eng 50:1121–1124
10. Katscher U, Voigt T, Findeklee C, Vernickel P, Nehrke K, Dössel O (2009) Determination of electric conductivity and local SAR via B1 mapping. IEEE Trans Med Imaging 28:1365–1374
11. Tha KK, Stehning C, Suzuki Y et al (2014) Noninvasive evaluation of electrical conductivity of the normal brain and brain tumors [abstract]. Proc Int Soc Magn Reson Med 22:1885
12. Voigt T, Katscher U, Doessel O (2011) Quantitative conductivity and permittivity imaging of the human brain using electric properties tomography. Magn Reson Med 66:456–466
13. Kim SY, Shin J, Kim DH et al (2016) Correlation between conductivity and prognostic factors in invasive breast cancer using magnetic resonance electric properties tomography (MREPT). Eur Radiol 26:2317–2326
14. Balidemaj E, de Boer P, van Lier AL et al (2016) In vivo electric conductivity of cervical cancer patients based on B_1^+ maps at 3T MRI. Phys Med Biol 61:1596–1607
15. Louis DN, Perry A, Reifenberger G et al (2016) The 2016 world health organization classification of tumors of the central nervous system: a summary. Acta Neuropathol 131:803–820
16. U.S. Food and Drug Administration (2014) Criteria for significant risk investigations of magnetic resonance diagnostic devices - guidance for industry and food and drug administration staff. U.S. Food and Drug Administration, Maryland. Available via https://www.fda.gov/RegulatoryInformation/Guidances/ucm072686.htm. Accessed 10 May 2017
17. Kang Y, Choi SH, Kim YJ et al (2011) Gliomas: Histogram analysis of apparent diffusion coefficient maps with standard- or high-b-value diffusion-weighted MR imaging–correlation with tumor grade. Radiology 261:882–890
18. Stogryn A (1971) Equations for calculating the dielectric constant of saline water. IEEE Trans Microwave Theory Tech 19:733–736
19. Kale VP, Patel SG, Gunjal PS et al (2012) Effect of repeated freezing and thawing on 18 clinical chemistry analytes in rat serum. J Am Assoc Lab Anim Sci 51:475–478
20. van Lier AL, Raaijmakers A, Voigt T et al (2014) Electrical properties tomography in the human brain at 1.5, 3, and 7T: a comparison study. Magn Reson Med 71:354–363
21. Turski PA, Houston LW, Perman WH et al (1987) Experimental and human brain neoplasms: detection with in vivo sodium MR imaging. Radiology 163:245–249
22. Simons M, Nave KA (2015) Oligodendrocytes: myelination and axonal support. Cold Spring Harb Perspect Biol 8:a020479
23. Tran P, Wong P, Sue A, Li Q, Carter P (2013) Influence of blood vessel conductivity in cochlear implant stimulation using a finite element head model [abstract]. Conf Proc IEEE Eng Med Biol Soc 2013:5291–5294
24. Runge VM, Schoerner W, Niendorf HP et al (1985) Initial clinical evaluation of gadolinium DTPA for contrast-enhanced magnetic resonance imaging. Magn Reson Imaging 3:27–35
25. Gupta RK, Cloughesy TF, Sinha U et al (2000) Relationships between choline magnetic resonance spectroscopy, apparent diffusion coefficient and quantitative histopathology in human glioma. J Neurooncol 50:215–226
26. Katscher U, Djamshidi K, Voigt T et al (2012) Estimation of breast tumor conductivity using parabolic phase fitting [abstract]. Proc Int Soc Magn Reson Med 20:3482